Functional redundancy of *Frizzled 3* and *Frizzled 6* in planar cell polarity control of mouse hair follicles

Bo Dong[1,2], Samantha Vold[1], Cristina Olvera-Jaramillo[1], and Hao Chang[1,2]

[1]Department of Dermatology, [2]Program in Genetics,
University of Wisconsin-Madison, Madison, Wisconsin 53706.

Keywords: planar cell polarity, skin, hair follicle, Fzd3, Fzd6, mouse development

Address for editorial correspondence:
Dr. Hao Chang
Department of Dermatology
University of Wisconsin-Madison
417 Medical Sciences Center
1300 University Avenue
Madison, WI 53706
Tel: 608-262-3602
E-mail: hchang@dermatology.wisc.edu

SUMMARY

The orientation of mouse hair follicles is controlled by the planar cell polarity (PCP) pathway. Mutations in PCP genes result in two categories of hair misorientation phenotype, randomly oriented and vertically oriented to the skin surface. Here we demonstrate that the randomly oriented hair phenotype in *Frizzled 6 (Fzd6)* is a partial loss of the polarity, due to the functional redundancy of another closely related Frizzled gene, *Fzd3*. Double knockout of *Fzd3* and *Fzd6* globally, or only in the skin, lead to vertically oriented hair follicles and a total loss of anterior-posterior polarity. Furthermore, we provide evidence that, contrary to the prevailing model, asymmetric localization of the Fzd6 protein is not observed in skin epithelial cells. Through transcriptome analyses and *in vitro* studies, we show collagen triple helix repeat containing 1 (Cthrc1) as a potential downstream effector of Fzd6, but not Fzd3. Cthrc1 binds directly to the extracellular domains of Fzd3 and Fzd6 to enhance the Wnt/PCP signaling. These results suggest that Fzd3 and Fzd6 play a redundant role in controlling the polarity of developing skin, but through non-identical mechanisms.

INTRODUCTION

The skin of mammals is a highly organized tissue with many structures in it exhibiting a precise orientation to the body axes. One apparent example is the hair, which is positioned at a fixed angle to the skin surface, rather than straight up. The orientation that each hair follicle extends from the dermis toward the skin surface is correlated to the body axes. For example, in the mouse back skin, all hair follicles point from anterior (head) to posterior (tail); on the limbs hair follicles point from proximal (body trunk) to distal (digits). In addition to hairs and hair follicles, many other structures in the skin are also polarized. For example, Merkel cell clusters, the epithelial derivatives that are involved in mechanosensation, are arranged in a semicircle around the base of the guard follicles with the opening of the semicircle always pointing toward the anterior head (Nurse and Diamond, 1984; Boulais and Misery, 2007; Maricich et al., 2009; Woo et al., 2010). Other hair follicle-associated structures, such as sebaceous glands, arrector pili muscles, and sensory nerve endings are also polarized in a direction that matches the central hair follicle (Wu et al., 2012; Chang and Nathans, 2013).

The orientation of mammalian skin structures and other surface structures in invertebrates and vertebrates are controlled by a conserved tissue polarity or planar cell polarity (PCP) system. Over 30 years of studies in *Drosophila* and mammals have revealed a core set of three membrane proteins that regulate PCP: Frizzled (Fzd), Strabismus (Stbm, Vangl in mammals), and Flamingo (Fmi, Celsr in mammals) (Wang and Nathans, 2007; Jenny, 2010; Goodrich and Strutt, 2011; Aw and Devenport, 2017; Butler and Wallingford, 2017). Mutations in all three families of PCP genes lead to aberrant hair orientations in mice: (1) Frizzled family - $Fzd6^{-/-}$ mice (Guo et al., 2004), (2) Vangl family - $Vangl2^{lp/lp}$ and *Vangl1/2* skin conditional knockout mice (Devenport and Fuchs, 2008; Chang et al., 2016), and (3) Celsr family - $Celsr1^{crsh/crsh}$ and *Celsr1* knockout mice (Devenport and Fuchs, 2008; Ravni et al., 2009). Interestingly, there appear to be two different types of hair follicle misorientation associated with PCP mutants: randomly oriented and oblique to the skin surface, as seen in the $Fzd6^{-/-}$ mice, and vertically oriented, as seen in the $Celsr1^{crsh/crsh}$, $Vangl2^{lp/lp}$, and *Vangl1/2* skin conditional knockout mice. It is still unclear whether the phenotype

differences between these two groups reflect the severities of follicle misorientation or distinct categories of polarity disruption.

Genetic analyses in *Drosophila* and mammals have identified many components of the PCP pathway and expanded our knowledge on the role of PCP genes in controlling tissue polarity. However, the mechanisms through which PCP integrates the global and local signal to orient diverse structures is still largely unknown. A widely accepted model of PCP signaling has emerged from studies in *Drosophila* wing epithelial cells, which involves the asymmetric localization of core PCP proteins to different sides of each cell (Wong and Adler, 1993; Usui et al., 1999; Lawrence et al., 2004; Chen et al., 2008; Strutt and Strutt, 2008; Wu and Mlodzik, 2009; Struhl et al., 2012). Frizzled proteins are enriched on the distal side of each cell, and Vang/Vangl proteins are enriched exclusively on the opposite proximal side. The multiple cadherin-domain proteins Fmi/Stan/Celsr are present on both sides of the cell. This asymmetric assembly of PCP complex (Frizzled versus Vangl) is hypothesized to create the polarity information across the tissue plane. Recently, studies in developing mouse skin appear to support the same model: prior to the polarization of mouse skin at embryonic day (E)14.5, Vangl2, Clesr1, and Fzd6 proteins are uniformly distributed at cell-cell borders; after the polarization of mouse skin at E15.5, PCP proteins are enriched on the anterior-posterior sides of epithelial cells and under-represented on the medial-lateral sides (Devenport and Fuchs, 2008). Furthermore, studies on transgenic mice mosaically expressing a GFP-Vangl2 fusion protein show that Vangl2 is enriched on the anterior side of the epithelial cells in polarized skins (Devenport et al., 2011). It is unknown whether Fzd6 is also asymmetrically localized in the epithelial cells to provide the vector information when the skin is polarized during development.

The present paper focuses on answering several open questions related to the role of one of the core PCP genes, *Fzd6*, in controlling skin polarity: (1) Is the random hair orientation in *Fzd6*$^{-/-}$ mice an intermediate/weaker phenotype compared to the vertically oriented hair follicles observed in other PCP mutant mice? We have found that hair follicles only partially lose the anterior-posterior polarity upon loss of *Fzd6*. *Fzd3*, a close homolog for *Fzd6*, is also expressed in the developing skin. Combined deletion of *Fzd3* and *Fzd6* results in vertically oriented hair follicles and a total loss of anterior-posterior polarity. (2) Is Fzd6 protein asymmetrically localized on the posterior side of the epithelial cells, as predicted by the *Drosophila* model? We have used genetic mosaic approaches to examine the subcellular localization of both endogenous and ectopically expressed Fzd6 proteins and found a consistent distribution of Fzd6 to all cell-cell borders. (3) What are the possible downstream effectors of Fzd6-induced signaling? Through Affymetrix gene chip analyses, we have identified collagen triple helix repeat containing 1 (Cthrc1) as one potential downstream effector of Fzd6. Cthrc1 directly binds to the extracellular domain of Fzd3 and Fzd6 and might promote skin polarity establishment by selectively enhancing the Wnt/PCP signaling pathway.

MATERIALS AND METHODS

Mouse lines and husbandry

The following mouse alleles were used: *Fzd6*$^{-/-}$ (Guo et al., 2004), *Fzd6*$^{CKO/CKO}$ (Chang et al., 2016), *Rosa26-LSL-Fzd6* (Hua et al., 2014), *K17-GFP* (Bianchi et al., 2005), *Fzd3*$^{+/-}$ (Wang et al., 2002), *Fzd3*$^{CKO/CKO}$ (Hua et al., 2013), *CAGG-CreER*^{TM} (Hayashi and McMahon, 2002), and *K14-Cre*

(Dassule et al., 2000). Mice were handled and housed according to the approved Institutional Animal Care and Use Committee (IACUC) protocol M005675 of the University of Wisconsin-Madison.

Immunostaining

For immunostaining of sagittal sections, embryos were embedded in OCT, fresh frozen, cryosectioned (14 μm) and fixed for 10 minutes in 4% formaldehyde in PBS. Sections were washed with PBST (0.1% Triton in PBS) for 10 minutes and blocked for one hour with 5% normal donkey or goat serum in PBST. Primary antibodies were incubated for two hours at room temperature or overnight at 4°C. The following primary antibodies were used: goat anti-Fzd6 (AF1526; R and D Systems; 1:400), rat anti-E-cadherin (ab11512-100; Abcam; 1:400), ZO-1 (61-7300; Lifetechnologies, 1:200), NCAM (MAB310; Millipore; 1:200), Keratin 5 (905501; BioLegend; 1:2000), and 3xHA (JH5604; 1:50,000). Secondary antibodies in PBST were incubated for one hour at room temperature. Secondary antibodies were Alexa Fluor 488-, 594-, or 647-conjugated donkey anti-goat, donkey anti-rat, or goat anti-rat IgG antibodies (Invitrogen; Grand Island, NY). Finally, sections were washed three times in PBST and mounted on slides with Fluoromount-G (Southern Biotech; Birmingham, AL). For whole-mount immunostaining of embryonic skins, embryos were fixed for one hour in 4% formaldehyde. Back skins were dissected, rinsed with PBS, washed with 0.3% PBST for 30 minutes, and incubated with primary antibodies in 0.3% PBST containing 5% normal goat or donkey serum overnight at 4°C. Skins were then washed in 0.3% PBST for 30 minutes three times, incubated in secondary antibodies in 0.3% PBST at room temperature for two hours, washed in 0.3% PBST and flat-mounted in Fluoromount G. Immunostained samples were imaged using Zeiss LSM500/700 confocal microscopes with Zen software.

Skin whole mounts

The procedures for preparation and processing of skin whole mounts for imaging of hair follicles based on melanin content were similar to previously described methods (Chang and Nathans, 2013; Chang et al., 2014). Dorsal back skins were dissected and flattened by pinning the edges to a flat Sylguard surface, fixed overnight in 4% paraformaldehyde in PBS, dehydrated through a graded alcohol series, and then clarified with benzyl benzoate: benzyl alcohol (BBBA) in a glass dish. Images were collected with a Zeiss Stemi 508 microscope with a color Axiocam 105 in combination with Zen software.

Plasmids and cell culture

Mouse Cthrc1 full-length cDNA was purchased from Open Biosystems (EMM1002-99258104, clone ID 40130184). A 3xHA tag was inserted at the very C-terminus by PCR, and the 3xHA-tagged Cthrc1 was subcloned into the pRK5 vector. 1D4-tagged mouse Fzd3 and Fzd6 plasmids were described before (Yu et al., 2012). To generate 1D4-tagged Fzd3 and Fzd6 with the extracellular domain deletion (Fzd3/6ΔN-1D4), PCR mutagenesis was used to delete amino acids between Leu^{25} to Arg^{203} and Leu^{21} to Lys^{199}, respectively. To generate 1D4-tagged Fzd3 and Fzd6 with the intracellular domain deletion (Fzd3/6ΔC-1D4), PCR mutagenesis was used to delete amino acids between Lys^{501} to Thr^{664} and Lys^{497} to Ser^{707}, respectively. All Clones were verified by sequencing. Standard procedures were used to transfect plasmid DNA into HEK293T grown in DMEM/F12 medium with 10% fetal bovine serum and penicillin/streptomycin. For each well of cells to be transfected in a 12 well tray, 0.5 μg of DNA was diluted in 50 μl of serum-free media

(SFM). 1.5 µl of FuGENE® HD Reagent (Promega) was added into the diluted DNA solution, mixed gently, and incubated for 10 minutes at room temperature before adding to the cells. For all mammalian cell transfections, cells were incubated for 48 hours post-transfection before assaying for protein/mRNA expression unless otherwise specified. Recombinant human Wnt3a, Wnt5a, and Wnt11 (R&D Systems, 5036-WN-010, 645-WN-010, and 6179-WN-010) were used at 100 ng/ml, LiCl (Fisher) at 20 mM.

Cell lysis, gel electrophoresis, co-immunoprecipitation assay, and immunoblotting

Transfected cells were lysed with 350 µl ice-cold lysis buffer (50 mM Tris-HCl pH 7.4, 150 mM NaCl, 1% Triton-X100 and 0.5% deoxycholate) supplemented with protease inhibitors (Roche, complete mini cocktail tablets). The cell lysates were incubated at 4°C for one hour, followed by centrifugation at 10,000xg for 5 minutes at 4°C. A total of 5 µl of the lysates was used as whole-cell lysates by adding 5 µl 2× SDS sample buffer. 50 µl HEK293T cell lysates were subjected to immunoprecipitation by incubation with 0.2 µl of anti-1D4 monoclonal antibody or 0.4 µl of anti-HA monoclonal antibody (Cell Signaling; 3724S) at 4°C overnight. Then, 30 µl Protein G Sepharose (GE Healthcare, 17-0618-01) was added to the lysates, which were further incubated at 4°C for 1 hour. Immune complexes were precipitated by centrifugation at 1,000 × g for 2 min, washed four times with 1 ml lysis buffer, and dissolved in 30 µl 2× SDS sample buffer. Immunoprecipitates or whole-cell lysates were resolved by SDS-PAGE on a 12.5%, 10% or 7.5% gel and blotted onto PVDF membranes (Millipore, IPFL0010). Immunoblots were incubated at 4°C overnight in the primary antibodies: rabbit anti-3xHA antiserum (JH5604, 1:250,000), mAb 1D4 ascites (Nathans Lab, 1:50,000), rabbit anti-active beta-catenin (Cell Signaling, #8814, 1:2000); the blots were then incubated with Li-Cor fluorescent secondary antibodies. Rho activation was assayed with the Rho Activation Kit (Cytoskeleton, BK036-S) following the manufacturer's instructions.

Microarray hybridization

Back skins were dissected from E15.5 *Fzd6*$^{+/-}$ and *Fzd6*$^{-/-}$ embryos. RNA was extracted using Trizol (Invitrogen) and RNeasy (Qiagen) kits. Three biologically independent sets of hybridizations were hybridized to Affymetrix mouse genome 430 2.0 microarrays and the data analyzed using Spotfire.

Semi-quantitative RT-PCR and quantitative real-time PCR (qRT-PCR)

cDNA synthesis was performed with GoScript reverse transcriptase (Promega, A5000) following the manufacturer's instructions. Quantitative real-time RT-PCR was performed in triplicate in 20 µl reactions with SYBR Premix Ex Taq II ROX plus (Takara, RR82LR) with 40 ng first-strand cDNA and 0.2 µg each forward and reverse primers. Samples were cycled once at 95 °C for 2 minutes, followed by 40 cycles of 95, 58, and 72 °C for 30 seconds each. Relative mRNA level was calculated using the ΔΔCT method with GAPDH as an endogenous control. Primers used for semi-quantitative RT-PCR and qRT-PCR were selected from the PrimerBank database (listed in **Table S1**).

Statistical analysis

Statistical analyses were performed with two-tailed unpaired Student's *t*-test between two experimental groups and one-way analysis of variance (ANOVA) for more than two experimental groups followed by Dunnett's or Tukey's test for multiple comparisons using the GraphPad Prism 7 software. The *P*-value less than 0.05 was considered as significant.

RESULTS

Partial loss of anterior-posterior polarity in hair follicles of *Fzd6*$^{-/-}$ mice

Previous studies have found that deletion of *Fzd6* either globally or specifically in the skin caused hair follicle misorientations in mouse embryos (Wang et al., 2010; Chang and Nathans, 2013; Chang et al., 2016). In *wild type* (*WT*) embryos, the early developing guard hair follicles on the back have parallel orientations, all pointing from the anterior (head) to the posterior (tail). In *Fzd6* mutants, the hair follicles on the back have uncorrelated orientations. This phenotype is very different from the one observed in other PCP mutants (including *Vangl2*$^{lp/lp}$, *Vangl1/2* skin conditional knockout, and *Celsr1*$^{crsh/crsh}$ mice), in which hair follicles are roughly perpendicular to the skin surface and lose the anterior-posterior polarity (Devenport and Fuchs, 2008; Chang et al., 2016). To determine whether individual misoriented hair follicles lose their polarity in *Fzd6*$^{-/-}$ mice, we collected back skins from E15.5 embryos, the time when guard hair follicles acquire the first sign of an anterior-to-posterior tilt, and performed whole-mount immunostaining with E-cadherin antibodies to examine the initial hair polarization. Consistent with the literature (Devenport and Fuchs, 2008), hair follicles in *WT* skin showed a uniform asymmetry: anterior cells expressing reduced levels of E-cadherin and adopt cell shapes distinct from posterior cells **(Fig. 1A)**. In *Fzd6*$^{-/-}$ skin, hair follicles were randomly oriented. In follicles with a tilted direction, either from anterior to posterior (same orientation as the anteroposterior axis), from posterior to anterior (a reversed orientation to the anteroposterior axis), or any other directions, hair follicles showed an asymmetry. The distribution of E-cadherin weak cells was closely correlated with the orientation of hair follicles (**Fig. 1B, D, and data not shown**). Interestingly, in hair follicles that point straight downward in the skin (about 30-40% of the follicles), this asymmetry in architecture was lost (**Fig. 1C**).

To determine whether the asymmetry of hair follicles maintains as hair follicles grow, we stained sagittal sections of back skin at E17.5 with makers for polarization, ZO-1 and NCAM (Devenport and Fuchs, 2008). As expected, we found that ZO-1 was highly expressed anteriorly in the lower germ, and NCAM was highly expressed posteriorly in the upper germ in *WT* skin (**Fig. 1E, I**). In *Fzd6*$^{-/-}$ skin, when follicles had an orientation from anterior to posterior, ZO-1 was highly expressed in the anterior compartment of the lower germ (**Fig. 1F**). In follicles with an orientation from posterior to anterior, ZO-1 was highly expressed in the posterior compartment (**Fig. 1H**). In follicles that point straight downward in the skin, ZO-1 was highly expressed in the middle compartment of the lower germ (**Fig. 1G**). These data suggest that the polarization of hair follicles still exists in E17.5 *Fzd6*$^{-/-}$ embryos, and the asymmetric distribution of ZO-1 correlates with the hair follicle orientation. Interestingly, NCAM was found at both the anterior and posterior sides of the upper germ in *Fzd6*$^{-/-}$ skin, no matter what direction the hair follicles pointed (**Fig. 1J-L**).

Together, these data suggest hair follicles in *Fzd6*$^{-/-}$ mice partially lose their anterior-posterior polarity.

Total loss of anterior-posterior polarity in hair follicles of *Fzd3/6* double knockout mice

There are ten *Fzd* genes in mammals, many of which are expressed in the developing skin (Reddy et al., 2004; Sennett et al., 2015). The partial loss of the anterior-posterior polarity in hair follicles of *Fzd6*$^{-/-}$ mice made us wonder whether other *Fzd* genes play a redundant role, especially *Fzd3*. *Fzd3* expression in the skin is undetectable at postnatal ages by a *Fzd3*^{lacZ} knock-in allele (Hua et al., 2014). However, its expression can be detected in the developing epidermis and hair follicles by RNA *in situ* hybridization and RT-PCR analyses (Hung et al., 2001; Reddy et al., 2004). To characterize the expression pattern of *Fzd3* in the skin in detail, we performed quantitative qRT-PCR on skin RNA at multiple developing time points. *Fzd3* transcripts were readily detected in skin RNA at E14.5, consistent with the earlier reports (Hung et al., 2001; Reddy et al., 2004). The expression level of *Fzd3* gradually increased over time and was 1.5-fold higher at postnatal day (P)3 than that of E14.5 (**Fig. 2A**). *Fzd6* expression in the developing skin did not change over time (**Fig. 2B**). Furthermore, there was no difference in *Fzd3* transcript levels between *WT* and *Fzd6*$^{-/-}$ samples, suggesting *Fzd3* expression is not affected by *Fzd6* deletion (**Fig. 2C**).

To determine whether *Fzd3* plays any complementary role to *Fzd6* in controlling skin polarity, we crossed *Fzd6*$^{-/-}$ mice to the *Fzd3*$^{+/-}$ background and generated *Fzd3/6* double knockout embryos (*Fzd3*$^{-/-}$;*Fzd6*$^{-/-}$). As previously reported, all *Fzd3*$^{-/-}$;*Fzd6*$^{-/-}$ embryos developed a fully open neural tube and died within minutes after birth (Wang et al., 2006). We collected back skins from E17.5 embryos and examined hair follicle orientations by staining the skin sagittal sections with Keratin 5 (K5) antibodies (**Fig. 2D**). While hair follicles in *WT* mice exhibited a tilted angle relative to the epithelial surface, knockout of both *Fzd3* and *Fzd6* led to vertically oriented hair follicles that resembled the phenotype observed in *Vangl2*$^{lp/lp}$, *Vangl1/2* skin conditional knockout, and *Celsr1*$^{crsh/crsh}$ mice. We also stained skin sections with ZO-1 and NCAM antibodies and found that both markers showed a symmetric pattern in *Fzd3/6* double knockout hair follicles, suggesting a total loss of anterior-posterior polarity (**Fig. 2E**). These data demonstrate that *Fzd3*/*6* act together in controlling hair follicle polarity. The fact that *Fzd3* single knockout mice did not show any obvious hair polarity phenotype (**Fig. S1**) suggests that *Fzd6* plays a greater role than *Fzd3* in patterning the skin.

Postnatal hair follicle refinement in mice with loss of both *Fzd3* and *Fzd6*

During the first postnatal week, hair follicles undergo a substantial refinement process which minimizes the angular difference among neighboring follicles (Wang et al., 2010; Cetera et al., 2017). By P8, most of the hair follicles in *Fzd6*$^{-/-}$ mice have aligned from a largely randomized orientation to a uniform anterior-to-posterior direction (Wang et al., 2010; Chang et al., 2015). The mechanism of this refinement is still unknown. To determine whether *Fzd3* plays a role in the hair follicle refinement process, we deleted *Fzd3* on the *Fzd6*$^{-/-}$ background using a conditional knockout allele of *Fzd3* (Hua et al., 2013) and the *Keratin14-Cre* (*K14-Cre*). The *K14-Cre* was used to selectively delete *Fzd3* in the epidermis starting around E12.5 to bypass the neonatal lethality in *Fzd3*$^{-/-}$;*Fzd6*$^{-/-}$ mice (Dassule et al., 2000; Chang et al., 2016). We observed that hair follicles in *Fzd3*$^{CKO/-}$;*Fzd6*$^{-/-}$;*K14-Cre* mice exhibited identical hair polarity phenotypes as *Fzd3*$^{-/-}$;*Fzd6*$^{-/-}$ mice, implying that *K14-Cre* acts sufficiently early to eliminate Fzd3-induced PCP

signaling in the developing epidermis (**Fig. S2**). *Fzd3$^{CKO/-}$;Fzd6$^{-/-}$;K14-Cre* mice were born at an expected ratio and survived without evidence of any obvious growth retardation, allowing us to study the postnatal hair refinement process in these mutants. At P8, hair follicles in *Fzd6$^{-/-}$* back skins exhibited limited deviations from the parallel anterior-to-posterior orientation of *WT* hair follicles (**Fig. 3A**). The combined loss of *Fzd3* and *Fzd6* in the epidermis produced a hair pattern that was indistinguishable from *Fzd6* single knockouts and *WT* mice (**Fig. 3B**). We did observe a sparse population of hair follicles (less than 20 follicles per animal) on the lower back of *Fzd3$^{CKO/-}$;Fzd6$^{-/-}$;K14-Cre* mice that still had uncorrelated orientations to their neighbors, which we did not see in the *Fzd6$^{-/-}$* mice. These uncorrelated hair follicles might still be in the process of rotating to their final orientation, perhaps due to a slightly slower refinement. Since most of the hair follicles in *Fzd3$^{CKO/-}$;Fzd6$^{-/-}$;K14-Cre* mice adopted an anterior-to-posterior direction at P8, similar to *Fzd6$^{-/-}$* mice, we concluded that *Fzd3* plays little or no role in hair reorientation during the refinement process.

Distribution of Fzd6 protein in skin epithelial cells

Asymmetric localization of PCP proteins to different sides of epithelial cells (proximal or distal, anterior or posterior) has been proposed as a mechanism to render tissue polarity in both *Drosophila* and mammals (Aw and Devenport, 2017; Butler and Wallingford, 2017). Surprisingly, at E15.5, we found that Fzd6 was uniformly distributed at cell-cell borders of the basal cell membranes (**Fig. 4A**). To determine the subcellular localization of Fzd6 with greater accuracy, we developed a strategy to induce mosaic expression of Fzd6 and examine its localization in individual skin epithelial cells (**Fig. 4B**). The *CAGG-CreER^{TM}* mice ubiquitously express a fusion protein of CreER, which enables tamoxifen-induced, Cre-mediated recombination (Hayashi and McMahon, 2002). We crossed *Fzd6$^{+/-}$;CAGG-CreER^{TM}* males with *Fzd6$^{CKO/CKO}$* females and injected pregnant females with low dosages of 4-hydroxytamoxifen (4-HT, 0.2 mg per animal) at E10.5 to induce mosaic recombination. Back skins from E15.5 embryos with the genotype of *Fzd6$^{CKO/-}$;CAGG-CreER^{TM}* were collected and stained using Fzd6 and E-cadherin antibodies (E-cadherin used to outline the plasma membrane). At this 4-HT dose, knockout cell patches comprising as few as 4 cells to more than 20 cells can be induced. In *WT* cells, the Fzd6 protein was observed on all sides of the plasma membrane, with no obvious enrichment along the anteroposterior axis or mediolateral axis (**Fig. 4C**). We quantified the fluorescence intensity on the anterior, posterior, and mediolateral borders (113 cells in 20 clones) and identified no significant difference in Fzd6 immunostaining intensity among these sides (**Fig. 4D**).

PCP can propagate from cell to cell through communication between neighboring cells. To exclude the possibility that the localization of Fzd6 in *WT* cells was affected by neighboring knockout cells, we took an overexpression approach. We induced mosaic expression of epitope-tagged Fzd6 in the skin using *Rosa26-LSL-Fzd6* mice. *Rosa26-LSL-Fzd6* is a conditional overexpression allele of *Fzd6* that we previously generated, in which ectopic expression of 3xHA-tagged Fzd6 can be induced in a Cre-dependent manner (Hua et al., 2014). We crossed *CAGG-CreER^{TM}* males with *Rosa26-LSL-Fzd6* females to obtain the *Rosa26-LSL-Fzd6;CAGG-CreER^{TM}* embryos. We induced mosaic Cre activity, harvested back skins, and performed whole-mount immunostaining in the same way as described in the previous section. The 3xHA antibody was used to detect the ectopic Fzd6 protein. We found that the localization pattern of ectopic Fzd6 protein was similar to what was observed in the mosaic knockout experiments – Fzd6 is on all sides of the plasma membrane (**Fig. 4E**). Quantification of the fluorescence intensity showed no

significant difference among the anterior, posterior, and mediolateral borders (102 cells in 12 clones). We also performed the mosaic deletion and overexpression experiments in E16.5 skin and observed similar immunostaining pattern of Fzd6 (**Fig. S3**). Together, these data suggest that Fzd6 is not asymmetrically distributed in the mouse skin epithelium.

Identifying Cthrc1 as a potential downstream effector of Fzd6

The hair follicle misorientation phenotype in *Fzd6*$^{-/-}$ mice appears to act through the PCP signaling system, but the downstream effectors of Fzd6 remain mysterious. In humans, *FZD6* loss-of-function mutations have been identified in several families with autosomal recessive nail dysplasia (Fröjmark et al., 2011). A follow-up histologic analysis in *Fzd6*$^{-/-}$ mice shows dysplastic claw development (Cui et al., 2013). Interestingly, transcriptome analysis identified many changes, including down-regulation of multiple claw-specific keratin genes, Wnt, bone morphogenetic protein, and Hedgehog genes. These data imply that Fzd6 signaling can function through regulating gene expression, at least in nail bed epithelial cells during mouse claw development. To search for potential downstream effectors of the Fzd6 signaling pathway in regulating hair follicle orientation, we profiled the transcriptomes of back skins from E15.5 *Fzd6*$^{+/-}$ and *Fzd6*$^{-/-}$ embryos by hybridization of three independent samples to Affymetrix MOE430 2.0 gene chips (**Fig. 5A**). As expected, *Fzd6* transcripts were substantially under-represented in the *Fzd6*$^{-/-}$ samples. In the *Fzd6*$^{+/-}$ versus *Fzd6*$^{-/-}$ comparison, about 50 genes exhibited greater than 1.5-fold abundance changes that were statistically significant (P <0.05) (**Fig. 5B**).

We next validated the Affymetrix gene chip data by qRT-PCR. Consistent with the chip hybridization data, we found the expression of *Fzd6*, *Cthrc1*, and *Serhl* was significantly reduced in E15.5 *Fzd6*$^{-/-}$ skins compared to control skins and the expression of *Krt13* and *Psca* was significantly increased. Three transcripts that exhibited a significant decline in the chip data - *Sdc2*, *6430550H21Rik*, and *Glipr2* (with estimated declines of ~2.1-fold, ~1.7-fold, and ~1.7-fold, respectively; **Fig. 5B, C**) - did not show statistically significant changes in *Fzd6*$^{-/-}$ skins by qRT-PCR. Among these genes with a validated expression level change, we focused on *Cthrc1* because it has been identified as a Wnt cofactor protein that selectively activates PCP pathway by stabilizing the Wnt-Frizzled/Ror2 complex *in vitro* (Yamamoto et al., 2008). We collected skin RNA from *Fzd6*$^{+/-}$ and *Fzd6*$^{-/-}$ mice at multiple development time points (E14.5, E15.5, E17.5, and P3) and performed qRT-PCR analysis on *Cthrc1*. We found the expression level of *Cthrc1* in the skin was consistently down-regulated upon *Fzd6* deletion (data not shown). Furthermore, we compared the expression level of *Cthrc1* in E17.5 *Fzd3*$^{-/-}$ versus *WT* back skins and found no significant difference, suggesting that either Cthrc1 is a specific downstream effector of Fzd6 or the transcriptional changes only occur when the PCP signaling intensity is near or below the threshold for polarization in the skin (**Fig. 5D**).

To test whether Fzd6 can directly regulate the expression of *Cthrc1*, we transiently transfected HEK293T cells with Fzd6 expression plasmids and harvested cells 2 days after transfection. *CTHRC1* expression levels were then analyzed by qRT-PCR. We chose HEK293T cells because the basal levels of *FZD6* and *CTHRC1* expression were undetectable in these cells (based on qRT-PCR, data not shown). As expected, the expression of *Fzd6* was dramatically increased in transfected HEK293T cells. However, the expression of *CTHRC1* was not significantly increased (**Fig. S4**). Adding recombinant Wnt ligands Wnt5a and Wnt11 also did not

change the *CTHRC1* expression level. These data suggest that Fzd6 is not sufficient to drive the expression of *CTHRC1* in HEK293T cells. We note that this assay might have uncertainties that limit its interpretation. For example, to activate the signaling pathway, Fzd6 might require additional proteins that are not present in HEK293T cells or if present, are too divergent for human proteins to interact with the expressed mouse Fzd6.

Cthrc1-Fzd3/6 binding promotes the activation of Wnt/PCP signaling

Cthrc1 can directly bind to several components of the Wnt signaling pathway, including Wnt ligands (Wnt3a, Wnt5a, and Wnt11), Frizzled receptors (Fzd3, Fzd5, and Fzd6), and the co-receptor Ror2, to form a stabilized complex (Yamamoto et al., 2008). Given the evidence that this complex involves both the ligand and receptors, we sought to determine whether the extracellular (N-terminal) domain of Frizzled receptors are required for the Cthrc1-Fzd binding. We made expression plasmids for 3xHA-tagged Cthrc1 (referred to as Cthrc1-3xHA) and 1D4-tagged Fzd3 or Fzd6 with the extracellular or intracellular domain deleted (referred to as Fzd3/6ΔN-1D4 and Fzd3/6ΔC-1D4, respectively). We transiently expressed these proteins in HEK293T cells and studied the domain requirement for binding using co-immunoprecipitation assay. Western blotting of the mutant Fzd3/6 proteins expressed in HEK293T cells following SDS-PAGE revealed a band at expected size, suggesting these tagged mutant proteins are stable (**Fig. 6B**). As expected, when we pulled down Cthrc1 with HA antibodies, we observed that Fzd3 and Fzd6 were co-precipitated. When we pulled down full-length Fzd3 and Fzd6 with 1D4 antibodies, we also observed that Cthrc1 was co-precipitated (**Fig. 6A**). Deletion of the N-terminal domain of Fzd3 and Fzd6 abolished the Cthrc1-Fzd binding, as Fzd3/6ΔN-1D4 failed to co-precipitate with Cthrc1. However, deletion of the C-terminal domain did not affect the Cthrc1-Fzd binding, as Fzd3/6ΔC-1D4 co-precipitated with Cthrc1 (**Fig. 6B**). These data suggest the N-terminal (extracellular) domains of Fzd3 and Fzd6 play a critical role in the Cthrc1-Fzd interaction.

Next, we investigated the effects of Cthrc1-Fzd3/6 binding on the activities of canonical Wnt and PCP signaling in HEK293T cells. For canonical Wnt signaling, we transfected cDNAs encoding Fzd3/6 with or without Cthrc1 and measured the activation of the canonical Wnt signaling by qRT-PCR on known downstream target genes. We found that co-expression of Cthrc1 and Fzd3/6 had no effects on the expression level of *LEF1*, and *AXIN2* (**Fig. S5**). Western blotting analysis on the lysates also showed no significant changes in the stabilization of beta-catenin (**Fig. 6C**). These data suggest that the basal level of canonical Wnt signaling in HEK293T cells is not significantly affected by Cthrc1-Fzd3/6. We performed similar experiments with the presence of recombinant Wnt3a protein and co-transfection of the canonical Wnt signaling coreceptor Lrp5. We found that Wnt3a/Lrp5 induced a significant increase in stabilization of beta-catenin (30% increase in the active form of beta-catenin, as compared to 110% increase in cells treated with 20 mM LiCl). Co-expression of Cthrc1 and Fzd3/6 caused no significant changes in the stabilization of beta-catenin that induced by Wnt3a/Lrp5 (**Fig. 6D**). Wnt3a/Lrp5 also induced upregulation of *LEF1* (17% by qRT-PCR, as compared to 76% in cells treated with 20 mM LiCl) and co-expression of Cthrc1 and Fzd3/6 did not change the expression level of *LEF1* (**Fig. S5**). These data suggest that the activation of canonical Wnt signaling induced by Wnt3a/Lrp5 in HEK293T cells is also not significantly affected by Cthrc1-Fzd3/6.

To test whether the Cthrc1-Fzd interaction can activate non-canonical Wnt signaling, we measured Rho activation using a pulldown assay in which Rho-GTP, but not Rho-GDP, is

selectively captured by the Rho-binding domain from rhotekin fused to glutathione-S-transferase. This experiment showed that Cthrc1 and Fzd6 alone increased the activation of RhoA and enhanced activation of RhoA was observed in co-expression of Cthrc1 with either Fzd3 or Fzd6 (**Fig. 6E**). The fact that Fzd6 transient transfection alone in HEK293T cells promotes RhoA activation (lane 4 vs. lane 1 in **Fig. 6E**) suggests that the ligand of Fzd6 is naturally present (e.g., Wnts produced by HEK293T cells). We next examined the endogenous expression level of all 19 *WNT* genes by semi-quantitative RT-PCR and found that several *WNT*s, including *WNT5A*, *WNT5B*, and *WNT10B*, are highly expressed in the HEK293T cells (**Fig. 6F**).

DISCUSSION

The experiments described here establish an essential role for *Fzd3* and *Fzd6* in controlling hair follicle polarity in mouse skin. In particular, we report that (1) *Fzd6* plays a major role and loss of *Fzd6* leads to a partial loss of the anterior-posterior polarity in hair follicles; (2) *Fzd3* plays a minor but supportive role, and loss of both *Fzd3* and *Fzd6* leads to a total loss of the anterior-posterior polarity in hair follicles; (3) asymmetric Fzd6 localization is not a mechanism to polarize the mouse skin; and (4) *Fzd6* knockout causes significant transcriptome changes and a positive feedback loop of Wnt/Fzd6-Cthrc1 might play a critical role in controlling skin polarity.

Models of Fzd3/6 signaling in controlling the polarity of hair follicles

All three core PCP gene families (Fzd, Vangl, and Celsr) have been shown to control hair follicle orientation (Guo et al., 2004; Devenport and Fuchs, 2008; Ravni et al., 2009). However, the hair follicle polarity defects are different among these PCP mutant mice. Hair follicles in *Vangl2*$^{lp/lp}$, *Vangl1/2* skin conditional knockout, and *Celsr1*$^{crsh/crsh}$ mice are oriented perpendicular to the skin plane, whereas *Fzd6*$^{-/-}$ mice are tilted. We found that hair follicles in *Fzd6*$^{-/-}$ mice still partially retain their anterior-posterior polarity and a combined loss of *Fzd3* and *Fzd6* causes a total loss of the polarity. These observations lead us to propose a threshold model for Frizzled signaling in controlling skin polarity (**Fig. 7**): the mouse skin receives PCP signaling by both Fzd3 and Fzd6 (Fzd6 plays a greater role than Fzd3) and their combined signaling intensity determines the fate of epithelial cells – polarized and aligned, partially polarized but randomly oriented, or non-polarized. For example, in *WT* skin, the combined signaling intensity of Fzd3 and Fzd6 is above the threshold for polarization, allowing for hair follicles to grow in an asymmetric tilt. In the *Fzd3* and *Fzd6* double knockout skin, the PCP signaling intensity is below the threshold for non-polarization, resulting in hair follicles to grow upright with symmetry. When the signaling intensity is in between the two thresholds, a partial loss of polarity can occur, as observed in *Fzd6*$^{-/-}$ mice. The observations that *Vangl1* single knockout does not affect skin polarity and mice with loss of both *Vangl1* and *Vangl2* have a more severe skin polarity phenotype than *Vangl2* single knockout mice support our threshold model (Chang et al., 2016; Cetera et al., 2017).

Frizzleds are the principal receptors for Wnt family of ligands (Bhanot et al., 1996). There are 10 mammalian Frizzled family members, which can be divided into five subfamilies based on the similarities in amino acid sequences and gene structures (Wang et al., 2016a). Functional redundancy has been found between Frizzled genes within the same subfamilies and even in different subfamilies (Wang et al., 2006; Yu et al., 2010; Ye et al., 2011; Yu et al., 2012). Fzd3 and Fzd6 are the most distant subfamily of Frizzled receptors, and they mainly function through

the non-canonical Wnt/PCP. Recent studies have identified that *Fzd3* and *Fzd6* play redundant roles in several developmental processes, including neural tube and eyelid closure, inner-ear sensory hair cell patterning, and lingual papillae patterning (Wang et al., 2006; Hua et al., 2014; Wang et al., 2016b). Our findings extend the concept of functional redundancy between *Fzd3* and *Fzd6* to the developing skin and hair follicles.

Asymmetric localization of membrane PCP proteins and polarity

Asymmetric distribution of membrane PCP proteins to different sides of a single cell is believed to be the hallmark of PCP establishment (Wang and Nathans, 2007; Goodrich and Strutt, 2011; Aw and Devenport, 2017; Butler and Wallingford, 2017). For example, in *Drosophila* wing epithelial cells, Stbm is localized to the proximal side, whereas Fzd is localized to the distal side. Fmi is localized at both the proximal and distal sides. These proteins form asymmetric cell-surface complexes together with their associated cytosolic proteins, and they convey the proximal-distal information from cell to cell within the epithelium. In the developing mouse back skin, Vangl2 has been reported to accumulate on the anterior side of the basal epithelial cells in transgenic mice that mosaically express GFP-Vangl2 fusion protein (Devenport et al., 2011). Whether Frizzled family proteins are also asymmetrically localized in the skin epithelium is unknown.

In the present studies, we took genetic sparse labeling approaches to examine the distribution of Fzd6 proteins in skin epithelium *in vivo* and surprisingly found no asymmetric localization of Fzd6 (to the posterior side of the cell, predicted by what is known in *Drosophila*). At E15.5, the Fzd6 protein was indeed enriched at cell-cell junctions in skin epithelial cells, but not on any side of the single cell (posterior, anterior, or mediolateral). These results contradict the model that Frizzled and Vangl proteins are localized to the opposite sides of the cell and convey polarity information. We speculate that either Fzd6 is asymmetrically modified in some manner that changes its activity (e.g., post-translational modifications), or Fzd6-associated protein(s) might establish the subcellular asymmetry. We interpret the data as a fundamental difference between *Drosophila* and mammalian PCP or among various tissue types. Different interactions and colocalizations of PCP proteins might contribute specifically to the development of polarity in a given tissue but not others. Observations that Fzd3/6 colocalize with Vangl2 at the surface of hair cells in the inner ear support our interpretation (Montcouquiol et al., 2006).

A positive feedback loop of Wnt/Fzd6-Cthrc1 in controlling hair follicle polarity

Among many transcriptional changes identified through non-biased transcriptome analysis in the developing skin upon the loss of Fzd6, we focused on Cthrc1, which is known to be a cofactor of non-canonical Wnt signaling (Yamamoto et al., 2008). We provided biochemical evidence that Cthrc1 can bind directly to the N-terminus of Fzd3 and Fzd6 and demonstrated that the binding between Cthrc1 and Fzd3/6 can enhance Fzd3/6-induced PCP signaling. We concluded, based on the functional analysis *in vitro*, that Cthrc1 is a potential downstream effector of Fzd6. Our *in vitro* data lead us to hypothesize that the major function of Cthrc1 in the skin is to enhance the Fzd3- and Fzd6-induced PCP signaling (model in **Fig. 7A**). It will be interesting to know whether *Cthrc1* mutant mice show any skin polarity defects or whether there are genetic interactions between *Fzd3/Fzd6* and *Cthrc1* in skin polarity control. In mice, it has been shown that *Cthrc1* genetically interacts with *Vangl2* as $Cthrc1^{LacZ/LacZ};Vangl2^{Lp/+}$ embryos display typical PCP phenotypes, including a neural tube closure defect in the midbrain region and misorientation

of the sensory hair cells in the cochlea (Yamamoto et al., 2008). How Cthrc1 interacts with Vangl2 or other core PCP proteins needs further investigation.

The observations that *Fzd3* plays a complementary role to *Fzd6* in controlling hair follicle polarity and several other developmental processes suggest that they induce a similar signaling cascade upon activation. However, it has been previously reported that ubiquitous overproduction of Fzd3 in mice can rescue *Fzd6*$^{-/-}$ phenotype but ubiquitous overproduction of Fzd6 can only partial rescue *Fzd3*$^{-/-}$ phenotype (Hua et al., 2014). The lack of total interchangeability could be due to functional differences between Fzd3 and Fzd6. Our finding that Cthrc1 is transcriptionally regulated by Fzd6 but not Fzd3 might be one manifestation of such signaling specificity. What accounts for the different activities of Fzd3 and Fzd6 is still unknown. As these two proteins share 50% amino acid identity in the N-terminal extracellular domain, 68% in the transmembrane domain, and less than 30% identity in the cytoplasmic C-terminal tail (Hua et al., 2014), generating chimeric proteins by domain swapping will be helpful to determine what region(s) might contribute to the functional specificity.

Acknowledgments. HC is supported by the startup funds from the University of Wisconsin-Madison and the Marjorie Hagan Endowed Professorship.

Author contributions. BD and HC designed experiments; BD, SV, COJ, and HC conducted experiments; BD, SV, and HC analyzed data and wrote the paper.

REFERENCES:

Aw, W. Y. and Devenport, D. (2017) 'Planar cell polarity: global inputs establishing cellular asymmetry', *Curr Opin Cell Biol* 44: 110-116.

Bhanot, P., Brink, M., Samos, C. H., Hsieh, J. C., Wang, Y., Macke, J. P., Andrew, D., Nathans, J. and Nusse, R. (1996) 'A new member of the frizzled family from Drosophila functions as a Wingless receptor', *Nature* 382(6588): 225-30.

Bianchi, N., Depianto, D., McGowan, K., Gu, C. and Coulombe, P. A. (2005) 'Exploiting the keratin 17 gene promoter to visualize live cells in epithelial appendages of mice', *Mol Cell Biol* 25(16): 7249-59.

Boulais, N. and Misery, L. (2007) 'Merkel cells', *J Am Acad Dermatol* 57(1): 147-65.

Butler, M. T. and Wallingford, J. B. (2017) 'Planar cell polarity in development and disease', *Nat Rev Mol Cell Biol* 18(6): 375-388.

Cetera, M., Leybova, L., Woo, F. W., Deans, M. and Devenport, D. (2017) 'Planar cell polarity-dependent and independent functions in the emergence of tissue-scale hair follicle patterns', *Dev Biol* 428(1): 188-203.

Chang, H., Cahill, H., Smallwood, P. M., Wang, Y. and Nathans, J. (2015) 'Identification of Astrotactin2 as a Genetic Modifier That Regulates the Global Orientation of Mammalian Hair Follicles', *PLoS Genet* 11(9): e1005532.

Chang, H. and Nathans, J. (2013) 'Responses of hair follicle-associated structures to loss of planar cell polarity signaling', *Proc Natl Acad Sci U S A* 110(10): E908-17.

Chang, H., Smallwood, P. M., Williams, J. and Nathans, J. (2016) 'The spatio-temporal domains of Frizzled6 action in planar polarity control of hair follicle orientation', *Dev Biol* 409(1): 181-93.

Chang, H., Wang, Y., Wu, H. and Nathans, J. (2014) 'Flat mount imaging of mouse skin and its application to the analysis of hair follicle patterning and sensory axon morphology', *J Vis Exp*(88): e51749.

Chen, W. S., Antic, D., Matis, M., Logan, C. Y., Povelones, M., Anderson, G. A., Nusse, R. and Axelrod, J. D. (2008) 'Asymmetric homotypic interactions of the atypical cadherin flamingo mediate intercellular polarity signaling', *Cell* 133(6): 1093-105.

Cui, C. Y., Klar, J., Georgii-Heming, P., Fröjmark, A. S., Baig, S. M., Schlessinger, D. and Dahl, N. (2013) 'Frizzled6 deficiency disrupts the differentiation process of nail development', *J Invest Dermatol* 133(8): 1990-7.

Dassule, H. R., Lewis, P., Bei, M., Maas, R. and McMahon, A. P. (2000) 'Sonic hedgehog regulates growth and morphogenesis of the tooth', *Development* 127(22): 4775-85.

Devenport, D. and Fuchs, E. (2008) 'Planar polarization in embryonic epidermis orchestrates global asymmetric morphogenesis of hair follicles', *Nat Cell Biol* 10(11): 1257-68.

Devenport, D., Oristian, D., Heller, E. and Fuchs, E. (2011) 'Mitotic internalization of planar cell polarity proteins preserves tissue polarity', *Nat Cell Biol* 13(8): 893-902.

Fröjmark, A. S., Schuster, J., Sobol, M., Entesarian, M., Kilander, M. B. C., Gabrikova, D., Nawaz, S., Baig, S. M., Schulte, G., Klar, J. et al. (2011) 'Mutations in Frizzled 6 cause isolated autosomal-recessive nail dysplasia', *Am J Hum Genet* 88(6): 852-860.

Goodrich, L. V. and Strutt, D. (2011) 'Principles of planar polarity in animal development', *Development* 138(10): 1877-92.

Guo, N., Hawkins, C. and Nathans, J. (2004) 'Frizzled6 controls hair patterning in mice', *Proc Natl Acad Sci U S A* 101(25): 9277-81.

Hayashi, S. and McMahon, A. P. (2002) 'Efficient recombination in diverse tissues by a tamoxifen-inducible form of Cre: a tool for temporally regulated gene activation/inactivation in the mouse', *Dev Biol* 244(2): 305-18.

Hua, Z. L., Chang, H., Wang, Y., Smallwood, P. M. and Nathans, J. (2014) 'Partial interchangeability of Fz3 and Fz6 in tissue polarity signaling for epithelial orientation and axon growth and guidance', *Development* 141(20): 3944-54.

Hua, Z. L., Smallwood, P. M. and Nathans, J. (2013) 'Frizzled3 controls axonal development in distinct populations of cranial and spinal motor neurons', *Elife* 2: e01482.

Hung, B. S., Wang, X. Q., Cam, G. R. and Rothnagel, J. A. (2001) 'Characterization of mouse Frizzled-3 expression in hair follicle development and identification of the human homolog in keratinocytes', *J Invest Dermatol* 116(6): 940-6.

Jenny, A. (2010) 'Planar cell polarity signaling in the Drosophila eye', *Curr Top Dev Biol* 93: 189-227.

Lawrence, P. A., Casal, J. and Struhl, G. (2004) 'Cell interactions and planar polarity in the abdominal epidermis of Drosophila', *Development* 131(19): 4651-64.

Maricich, S. M., Wellnitz, S. A., Nelson, A. M., Lesniak, D. R., Gerling, G. J., Lumpkin, E. A. and Zoghbi, H. Y. (2009) 'Merkel cells are essential for light-touch responses', *Science* 324(5934): 1580-2.

Montcouquiol, M., Sans, N., Huss, D., Kach, J., Dickman, J. D., Forge, A., Rachel, R. A., Copeland, N. G., Jenkins, N. A., Bogani, D. et al. (2006) 'Asymmetric localization of Vangl2 and Fz3 indicate novel mechanisms for planar cell polarity in mammals', *J Neurosci* 26(19): 5265-75.

Nurse, C. A. and Diamond, J. (1984) 'A fluorescent microscopic study of the development of rat touch domes and their Merkel cells', *Neuroscience* 11(2): 509-20.

Ravni, A., Qu, Y., Goffinet, A. M. and Tissir, F. (2009) 'Planar cell polarity cadherin Celsr1 regulates skin hair patterning in the mouse', *J Invest Dermatol* 129(10): 2507-9.

Reddy, S. T., Andl, T., Lu, M. M., Morrisey, E. E. and Millar, S. E. (2004) 'Expression of Frizzled genes in developing and postnatal hair follicles', *J Invest Dermatol* 123(2): 275-82.

Sennett, R., Wang, Z., Rezza, A., Grisanti, L., Roitershtein, N., Sicchio, C., Mok, K. W., Heitman, N. J., Clavel, C., Ma'ayan, A. et al. (2015) 'An Integrated Transcriptome Atlas of Embryonic Hair Follicle Progenitors, Their Niche, and the Developing Skin', *Dev Cell* 34(5): 577-91.

Struhl, G., Casal, J. and Lawrence, P. A. (2012) 'Dissecting the molecular bridges that mediate the function of Frizzled in planar cell polarity', *Development* 139(19): 3665-74.

Strutt, H. and Strutt, D. (2008) 'Differential stability of flamingo protein complexes underlies the establishment of planar polarity', *Curr Biol* 18(20): 1555-64.

Usui, T., Shima, Y., Shimada, Y., Hirano, S., Burgess, R. W., Schwarz, T. L., Takeichi, M. and Uemura, T. (1999) 'Flamingo, a seven-pass transmembrane cadherin, regulates planar cell polarity under the control of Frizzled', *Cell* 98(5): 585-95.

Wang, Y., Chang, H. and Nathans, J. (2010) 'When whorls collide: the development of hair patterns in frizzled 6 mutant mice', *Development* 137(23): 4091-9.

Wang, Y., Chang, H., Rattner, A. and Nathans, J. (2016a) 'Frizzled Receptors in Development and Disease', *Curr Top Dev Biol* 117: 113-39.

Wang, Y., Guo, N. and Nathans, J. (2006) 'The role of Frizzled3 and Frizzled6 in neural tube closure and in the planar polarity of inner-ear sensory hair cells', *J Neurosci* 26(8): 2147-56.
Wang, Y. and Nathans, J. (2007) 'Tissue/planar cell polarity in vertebrates: new insights and new questions', *Development* 134(4): 647-58.

Wang, Y., Thekdi, N., Smallwood, P. M., Macke, J. P. and Nathans, J. (2002) 'Frizzled-3 is required for the development of major fiber tracts in the rostral CNS', *J Neurosci* 22(19): 8563-73.

Wang, Y., Williams, J., Rattner, A., Wu, S., Bassuk, A. G., Goffinet, A. M. and Nathans, J. (2016b) 'Patterning of papillae on the mouse tongue: A system for the quantitative assessment of planar cell polarity signaling', *Dev Biol* 419(2): 298-310.

Wong, L. L. and Adler, P. N. (1993) 'Tissue polarity genes of Drosophila regulate the subcellular location for prehair initiation in pupal wing cells', *J Cell Biol* 123(1): 209-21.

Woo, S. H., Stumpfova, M., Jensen, U. B., Lumpkin, E. A. and Owens, D. M. (2010) 'Identification of epidermal progenitors for the Merkel cell lineage', *Development* 137(23): 3965-71.

Wu, H., Williams, J. and Nathans, J. (2012) 'Morphologic diversity of cutaneous sensory afferents revealed by genetically directed sparse labeling', *Elife* 1: e00181.

Wu, J. and Mlodzik, M. (2009) 'A quest for the mechanism regulating global planar cell polarity of tissues', *Trends Cell Biol* 19(7): 295-305.

Yamamoto, S., Nishimura, O., Misaki, K., Nishita, M., Minami, Y., Yonemura, S., Tarui, H. and Sasaki, H. (2008) 'Cthrc1 selectively activates the planar cell polarity pathway of Wnt signaling by stabilizing the Wnt-receptor complex', *Dev Cell* 15(1): 23-36.

Ye, X., Wang, Y., Rattner, A. and Nathans, J. (2011) 'Genetic mosaic analysis reveals a major role for frizzled 4 and frizzled 8 in controlling ureteric growth in the developing kidney', *Development* 138(6): 1161-72.

Yu, H., Smallwood, P. M., Wang, Y., Vidaltamayo, R., Reed, R. and Nathans, J. (2010) 'Frizzled 1 and frizzled 2 genes function in palate, ventricular septum and neural tube closure: general implications for tissue fusion processes', *Development* 137(21): 3707-17.

Yu, H., Ye, X., Guo, N. and Nathans, J. (2012) 'Frizzled 2 and frizzled 7 function redundantly in convergent extension and closure of the ventricular septum and palate: evidence for a network of interacting genes', *Development* 139(23): 4383-94.

Figures

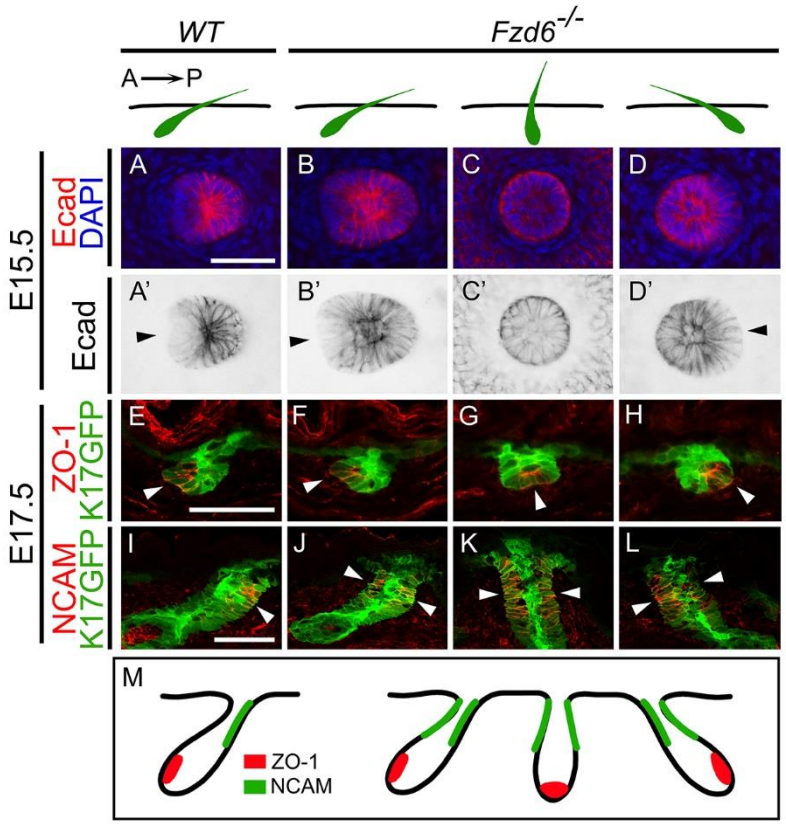

Figure 1. Partial loss of anterior-posterior polarity in *Fzd6*$^{-/-}$ hair follicles.

Top, diagrams showing the sectional view of hair follicles (green) in *WT* and *Fzd6*$^{-/-}$ skin. In *WT* skin, hair follicles extend from dermis to the skin surface, all pointing from anterior to posterior. In *Fzd6*$^{-/-}$ skin, the orientations of hair follicles are nearly randomized.

(A-D, A'-D'), whole-mount immunostaining of E15.5 back skins with E-cadherin (Ecad) antibodies. Hair follicles in *WT* skin show a titled angle, anterior cells have reduced levels of E-cadherin and adopt shapes different from posterior cells. Hair follicles in *Fzd6*$^{-/-}$ skin show a combination of different orientations.

(E-L), sagittal sections of E17.5 back skins stained with an anterior marker ZO-1 (E-H) or a posterior marker NCAM (I-L). Hair follicles are visualized by the fluorescence of a *K17GFP* transgene (green). (M), diagrams showing the asymmetric distribution of ZO-1 and NCAM in *WT* hair follicles (left) and the asymmetry of NCAM is lost in *Fzd6*$^{-/-}$ hair follicles (right).

A-P, anterior-to-posterior. Scale bar, 50 μm.

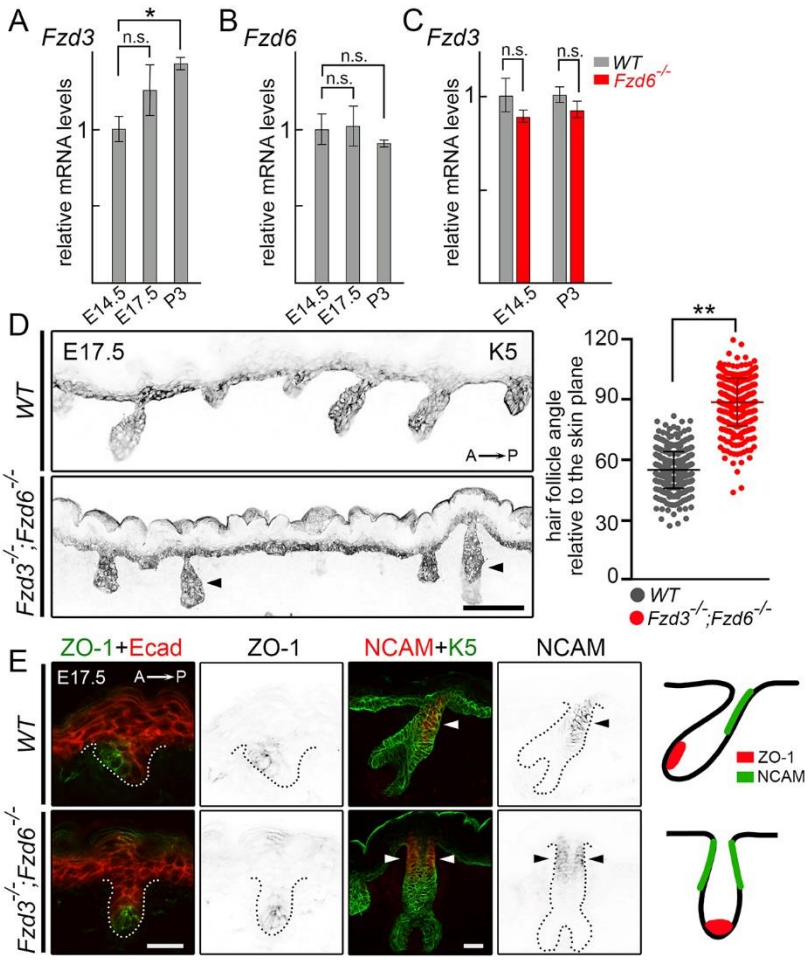

Figure 2. *Fzd3* and *Fzd6* act redundantly in controlling hair follicle polarity.

(A) Expression of *Fzd3* in *WT* skins by qRT- PCR.

(B) Expression of *Fzd6* in *WT* skins by qRT- PCR.

(C) Expression of *Fzd3* in *WT* and *Fzd6*$^{-/-}$ skin by qRT- PCR.

All data represent mean ± SEM of three biological replicates. *GAPDH* was used as a control. In panels A and B, the mRNA expression levels of *Fzd3* and *Fzd6* in E17.5 and P3 back skins were compared to E14.5 skins using ANOVA followed by Dunnett's multiple comparison test. In Panel C, the *Fzd3* expression levels in *WT* and *Fzd6* KO skins were compared using the Student's t-test at both time points (*, $P < 0.05$; n.s., not significant).

(D) Epithelial cells and developing hair follicles were visualized by Keratin 5 (K5) immunostaining on sagittal sections of E17.5 back skins. In the absence of both *Fzd3* and *Fzd6*, hair follicles are vertically oriented. Hair follicle angles to the plane of the skin were compared using the Student's t-test. *WT*, n = 456 hair follicles; *Fzd3*$^{-/-}$;*Fzd6*$^{-/-}$, n = 402 hair follicles (**, $P <$ 0.01).

(E) Complete loss of A-P polarity in *Fzd3*$^{-/-}$;*Fzd6*$^{-/-}$ hair follicles. Sagittal sections of E17.5 back skins stained with an anterior marker ZO-1 (left panels) or posterior marker NCAM (middle panels). Ecad and K5 antibodies were used to highlight skin epithelia and hair follicles. White dotted lines outline the hair follicles. Diagrams showing the asymmetric distribution of ZO-1 and NCAM in *WT* hair follicles and the complete loss of A-P polarity in *Fzd3*$^{-/-}$;*Fzd6*$^{-/-}$ hair follicles (right panels).

A-P, anterior-to-posterior. Scale bars, 100 μm in D and 25 μm in E.

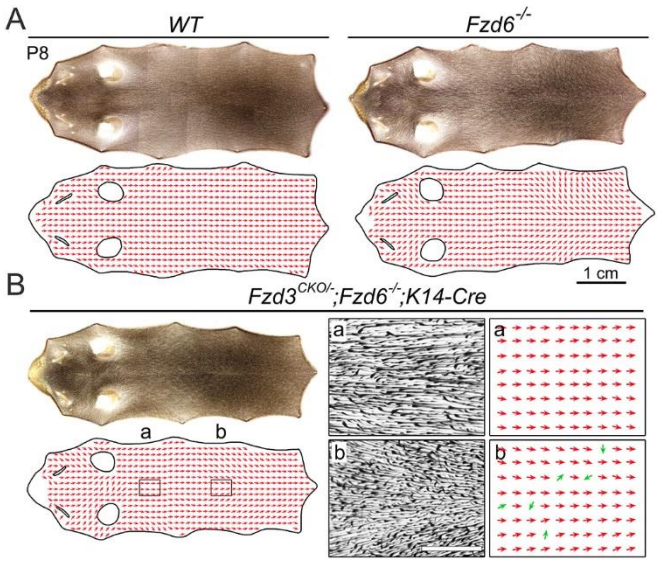

Figure 3. Global patterns of hair follicle orientation in back skins of *WT*, *Fzd6*$^{-/-}$, and *Fzd3*$^{CKO/-}$*;Fzd6*$^{-/-}$*;K14-Cre* mice at P8.

Montage of images of back skin flat mounts and the corresponding vector maps, anterior is to the left, and posterior is to the right. Vector maps are constructed by sampling hair follicle orientations at each point on the vector grid using a similar method described previously (Chang et al., 2015). The two narrow openings in vector maps mark the locations of eyes, and the two round openings mark the locations of the ears.

(A) *WT* and *Fzd6*$^{-/-}$ skin.

(B) *Fzd3*$^{CKO/-}$*;Fzd6*$^{-/-}$*;K14-Cre* skin. Images a and b correspond to the boxed regions in the adjacent vector maps. Green arrows in b highlight the hair follicles that have uncorrelated orientations to their neighbors.

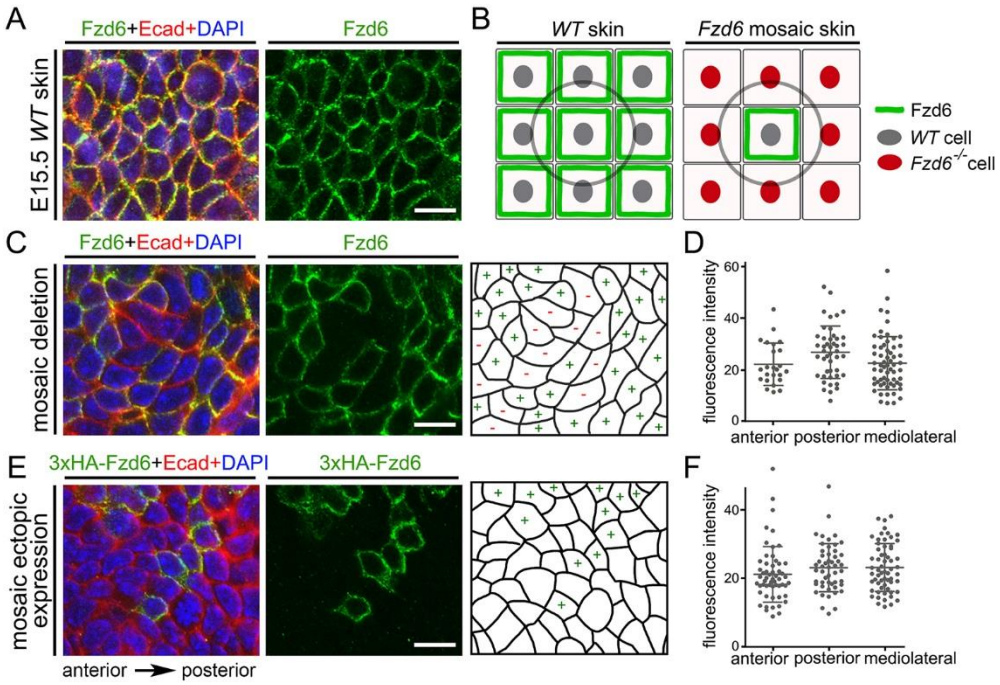

Figure 4. Localization of Fzd6 in individual skin epithelial cells by genetic mosaic labeling.

(A) Whole-mount immunostaining of E15.5 *WT* back skins with Fzd6 and E-cadherin antibodies.

(B) Diagrams showing the strategy to visualize the localization of Fzd6 in individual skin epithelial cells. Flat-mount view of nine cells are shown. The cell in the middle (circled) is used to determine the localization of the Fzd6 protein.

(C) Mosaic expression of Fzd6 was induced in *Fzd6*$^{CKO/-}$*;CAGG-CreER*^{TM} embryos treated with 4-HT at E10.5. E15.5 back skins were collected and stained with Fzd6 (green) and E-cadherin (red) antibodies. The right panel shows the schematic of the *Fzd6* (+) versus *Fzd6* (-) cells.

(D) Quantification of fluorescence intensity on anterior, posterior, and mediolateral sides of the cells at the borders of *Fzd6* (+) and *Fzd6* (-) clones.

(E) Mosaic expression of 3xHA-tagged Fzd6 on a *WT* background was induced in *Rosa26-LSL-Fzd6;CAGG-CreER*^{TM} embryos treated with 4-HT at E10.5. E15.5 back skins were collected and stained with 3xHA (green) and E-cadherin (red) antibodies. The right panel shows the schematic of the *3xHA-Fzd6* (+) versus *WT* cells.

(F) Quantification of fluorescence intensity on anterior, posterior, and mediolateral sides of the cells at the borders of *3xHA-Fzd6* (+) and *WT* clones.

Anterior is to the left and posterior to the right. Scale bar, 10 μm.

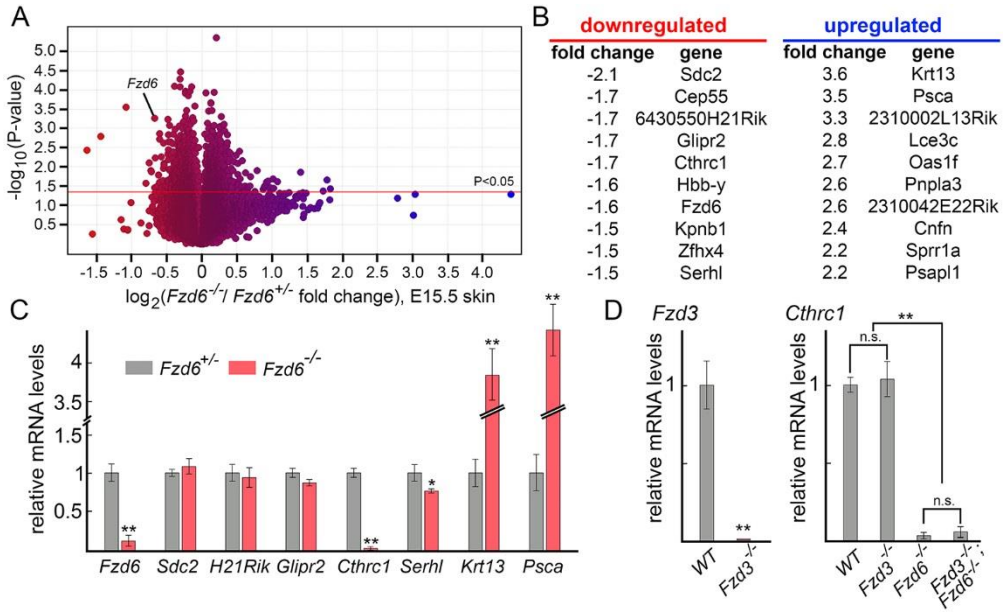

Figure 5. Identification of Cthrc1 as a potential downstream effector of Fzd6.

(A) Transcriptome changes in response to the loss of *Fzd6*. Mouse MOE430 2.0 Affymetrix arrays were hybridized in three biologically independent experiments with RNA from E15.5 *Fzd6*$^{+/-}$ and *Fzd6*$^{-/-}$ back skins. As expected, the probe set representing *Fzd6* transcripts shows reduced hybridization with RNA from *Fzd6*$^{-/-}$ skins. Blue, up-regulated; red, down-regulated expression.

(B) Lists of top ten genes with the highest fold change, including both up- and down-regulated genes.

(C) Validation of the Affymetrix gene chip data by qRT-PCR using RNA extracted from E15.5 *Fzd6*$^{+/-}$ and *Fzd6*$^{-/-}$ back skins.

(D) Expression of *Cthrc1* in the skin is not affected by *Fzd3* deletion.

All data represent mean ± SEM of three biological replicates. *GAPDH* was used as a control. Quantification of data between two groups was compared using the Student's t-test. The expression levels of *Cthrc1* in panel D were compared using ANOVA followed by Tukey's test (*, $P < 0.05$; **, $P < 0.01$; n.s., not significant).

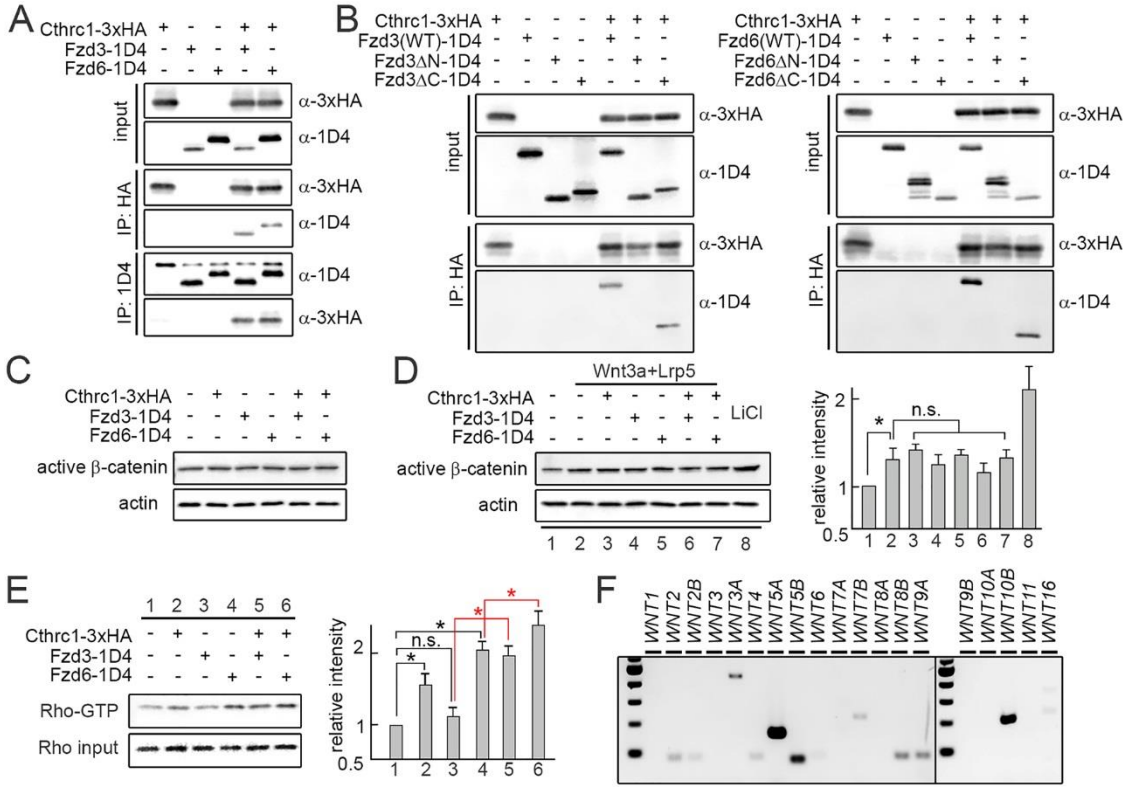

Figure 6. Effects of Cthrc1-Fzd3/6 on canonical and PCP signaling.

(A) Binding of Cthrc1 and Fzd3/6 *in vitro*. Protein extracts from HEK293T cells expressing 1D4-tagged Fzd3 or Fzd6, with or without 3xHA-Cthrc1, were pulled-down with either anti-HA or anti-1D4 antibodies. Both 1D4-Fzd3 and 1D4-Fzd6 co-immunoprecipitate with 3xHA-Cthrc1, and vice versa.

(B) Domain requirements of Fzd3/6 for their binding to Cthrc1. Deletion of the N-terminal domain of Fzd3 and Fzd6 abolishes the Cthrc1-Fzd binding, as Fzd3/6ΔN-1D4 fail to co-precipitate with Cthrc1. However, deletion of the C-terminal domain does not affect the Cthrc1-Fzd binding, as Fzd3/6ΔC-1D4 still co-precipitate with Cthrc1. These data suggest the N-terminal (extracellular) domains of Fzd3 and Fzd6 is required for the Cthrc1-Fzd interactions.

(C) Cthrc1-Fzd3/6 does not affect the basal level of beta-catenin activation in HEK293T cells, as Western blotting shows no changes in the active form of beta-catenin level in transiently transfected HEK293T cells. Actin as a control.

(D) Cthrc1-Fzd3/6 does not affect the beta-catenin activation induced by Wnt3a. Cells treated with 20 mM LiCl were used as a positive control.

(E) Increase in RhoA activation in transiently transfected HEK293T cells with Cthrc1 or Fzd6 (2, 4 vs. 1), but not Fzd3 (3 vs. 1). A synergistic effect between Fzd3/6 and Cthrc1 in RhoA activation is observed (5 vs. 3, 6 vs. 4). Experiments were performed three times in D and E, and the quantification data represent mean ± SEM. Quantification of data was compared using ANOVA followed by Tukey's t-test (*, $P < 0.05$; n.s., not significant).

(F) Endogenous expression of *WNT*s in HEK293T cells. Among 19 *WNT*s, *WNT5A*, *WNT5B*, and *WNT10B* are expressed at a high level, as assessed by RT-PCR.

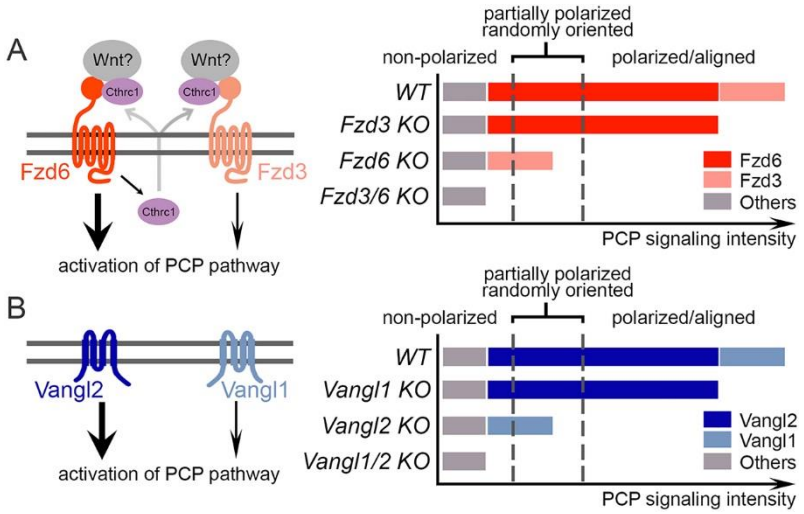

Figure 7. A threshold model of PCP signaling intensity and polarity outcomes in the developing skin.

(A) Left, models of Fzd3/6 signaling. Both Fzd3 and Fzd6 can induce activation of the PCP pathway. Cthrc1, the cofactor that enhances Wnt/PCP signaling, is a potential downstream effector of Fzd6. Right, the threshold model of PCP signaling intensity in determining the polarity outcomes of developing mouse skin. Black dotted lines indicate two thresholds – non-polarization and polarization (see text for details). Dark red bar, PCP signaling contributed by Fzd6; light red bar, PCP signaling contributed by Fzd3; gray bar, PCP signaling contributed by others. Note that Fzd6 plays a major role compared to Fzd3.

(B) Models of Vangl1/2 signaling. Both Vangl1 and Vangl2 can induce activation of the PCP pathway, but Vangl2 plays a major role compared to Vangl1. Similar to Fzd3/6, the combined signaling intensity of Vangl1 and Vangl2 determines the fate of epithelial cells. Dark blue bar, PCP signaling contributed by Vangl2; light blue bar, PCP signaling contributed by Vangl1; gray bar, PCP signaling contributed by others.

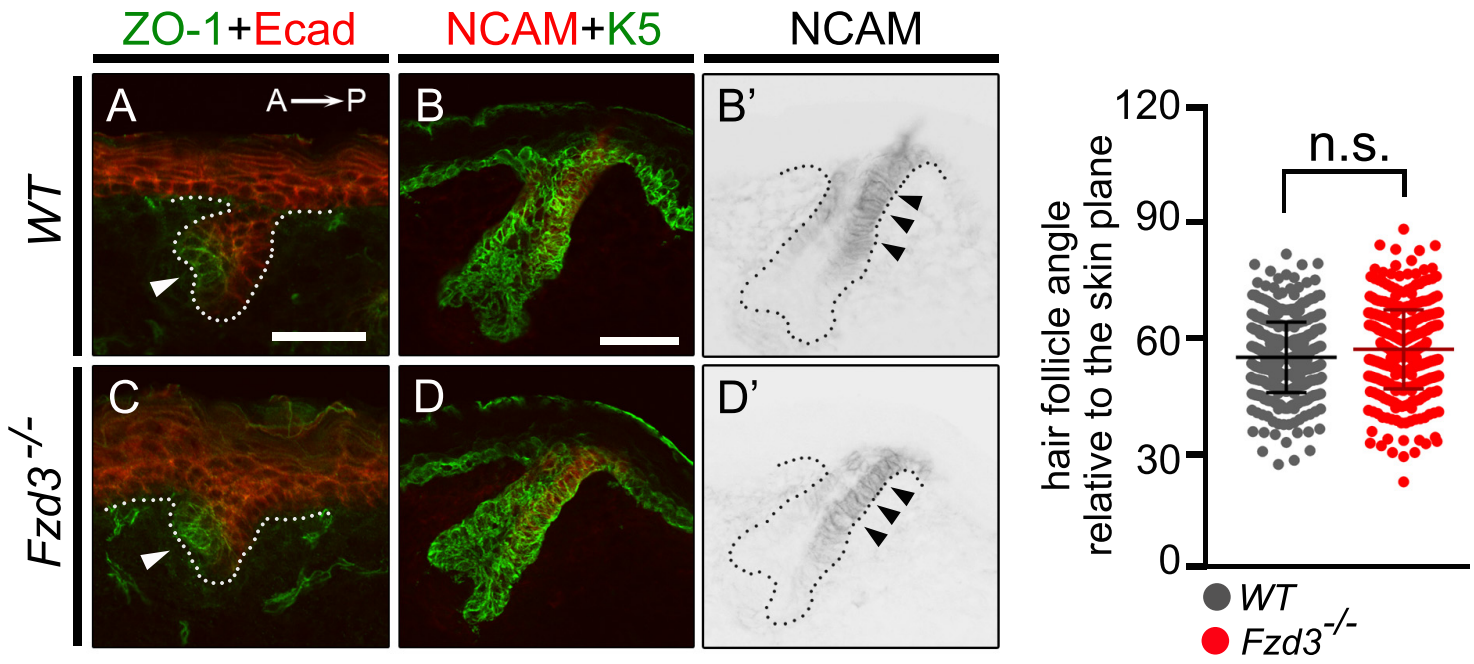

Figure S1. Loss of *Fzd3* does not affect hair follicle polarity.

Left, sagittal sections of E17.5 back skins stained with an anterior marker ZO-1 or posterior marker NCAM. E-cadherin and K5 antibodies were used to highlight skin epithelia and hair follicles. Anterior is to the left, and posterior is to the right. Scale bar, 50 μm. Dotted lines outline the hair follicles.

Right, hair follicle angles to the plane of the skin were compared using the Student's t-test. *WT*, n = 456 hair follicles; *Fzd3*$^{-/-}$, n = 408 hair follicles (n.s., not significant).

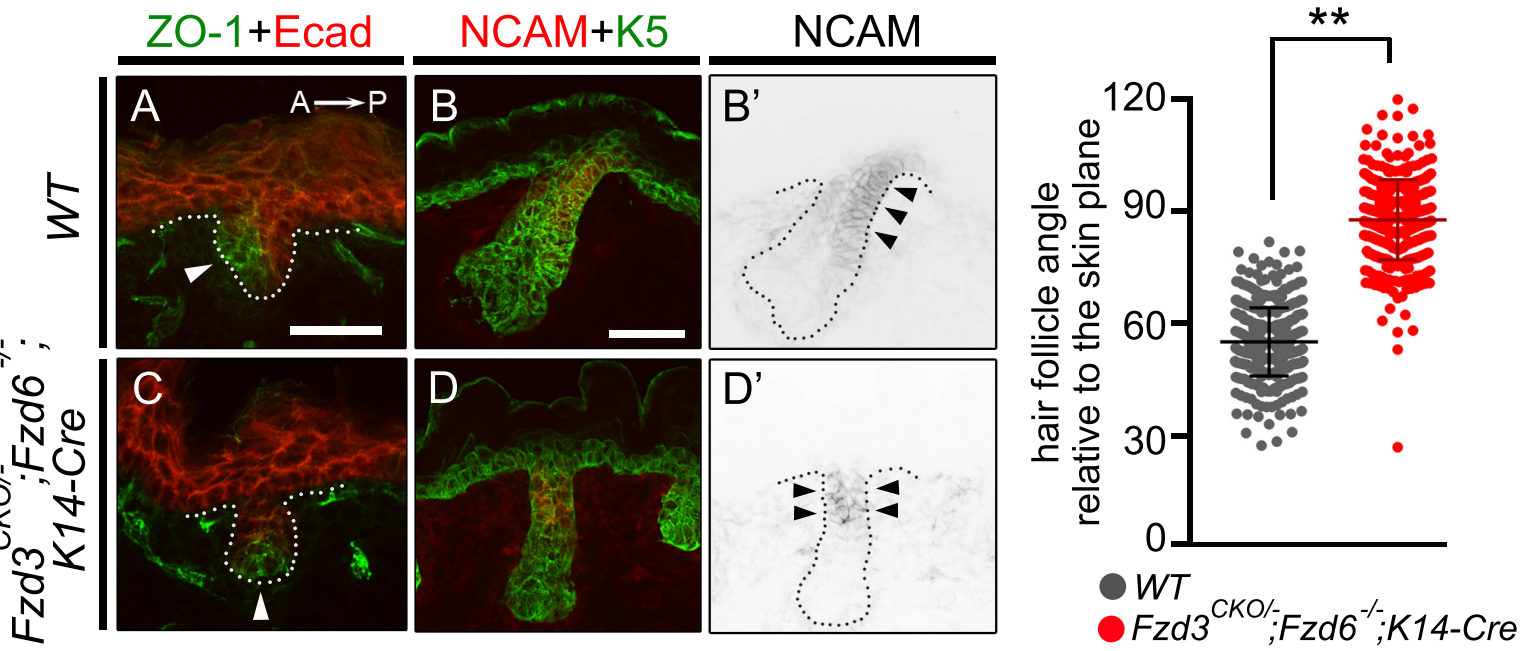

Figure S2. Conditional knockout of *Fzd3* using K14-Cre on *Fzd6*$^{-/-}$ background recapitulates the skin phenotype of *Fzd3*$^{-/-}$;*Fzd6*$^{-/-}$ mice.

Left, sagittal sections of E17.5 back skins stained with an anterior marker ZO-1 or posterior marker NCAM. E-cadherin and K5 antibodies were used to highlight skin epithelia and hair follicles. In *Fzd3*$^{CKO/-}$;*Fzd6*$^{-/-}$;*K14-Cre* skin, hair follicles are perpendicular to the skin surface, and the asymmetric localization of ZO-1 and NCAM is lost (similar to *Fzd3*$^{-/-}$;*Fzd6*$^{-/-}$ mice). Anterior is to the left, and posterior is to the right. Scale bar, 50 µm. Dotted lines outline the hair follicles.

Right, hair follicle angles to the plane of the skin were compared using the Student's t-test. *WT*, n = 456 hair follicles; *Fzd3*$^{CKO/-}$;*Fzd6*$^{-/-}$;*K14-Cre*, n = 431 hair follicles (**, $P < 0.01$).

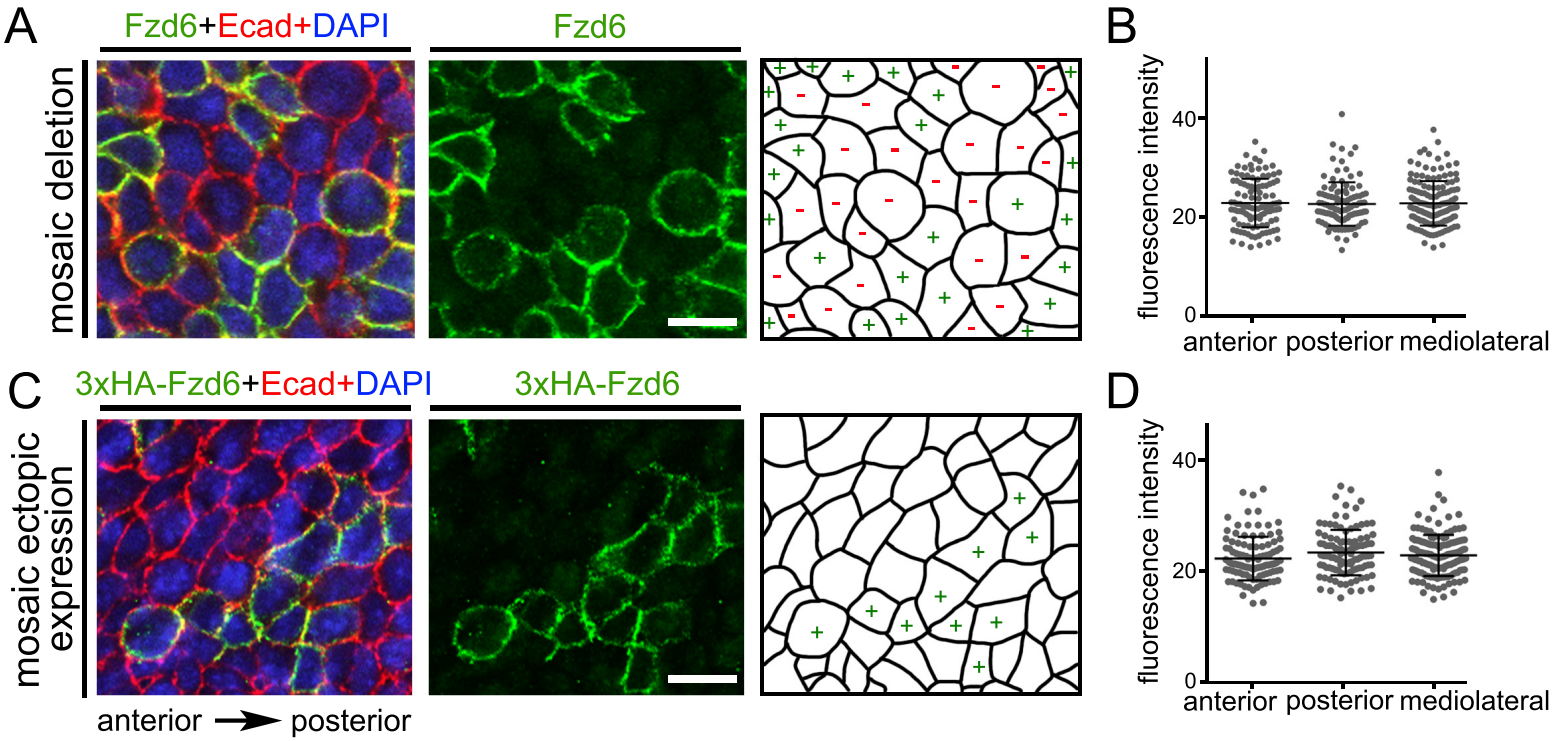

Figure S3. Localization of Fzd6 in individual skin epithelial cells at E16.5 by genetic mosaic labeling.

(A) Mosaic expression of Fzd6 was induced in *Fzd6*$^{CKO/-}$*;CAGG-CreER*^{TM} embryos treated with 4-HT at E10.5. E16.5 back skins were collected and stained with Fzd6 (green) and E-cadherin (red) antibodies. The right panel shows the schematic of the *Fzd6* (+) versus *Fzd6* (-) cells.

(B) Quantification of fluorescence intensity on anterior, posterior, and mediolateral sides of the cells at the borders of *Fzd6* (+) and *Fzd6* (-) clones.

(C) Mosaic expression of 3xHA-tagged Fzd6 on a *WT* background was induced in *Rosa26-LSL-Fzd6;CAGG-CreER*^{TM} embryos treated with 4-HT at E10.5. E16.5 back skins were collected and stained with 3xHA (green) and E-cadherin (red) antibodies. The right panel shows the schematic of the *3xHA-Fzd6* (+) versus *WT* cells.

(D) Quantification of fluorescence intensity on anterior, posterior, and mediolateral sides of the cells at the borders of *3xHA-Fzd6* (+) and *WT* clones.

Anterior is to the left and posterior to the right. Scale bar, 10 μm.

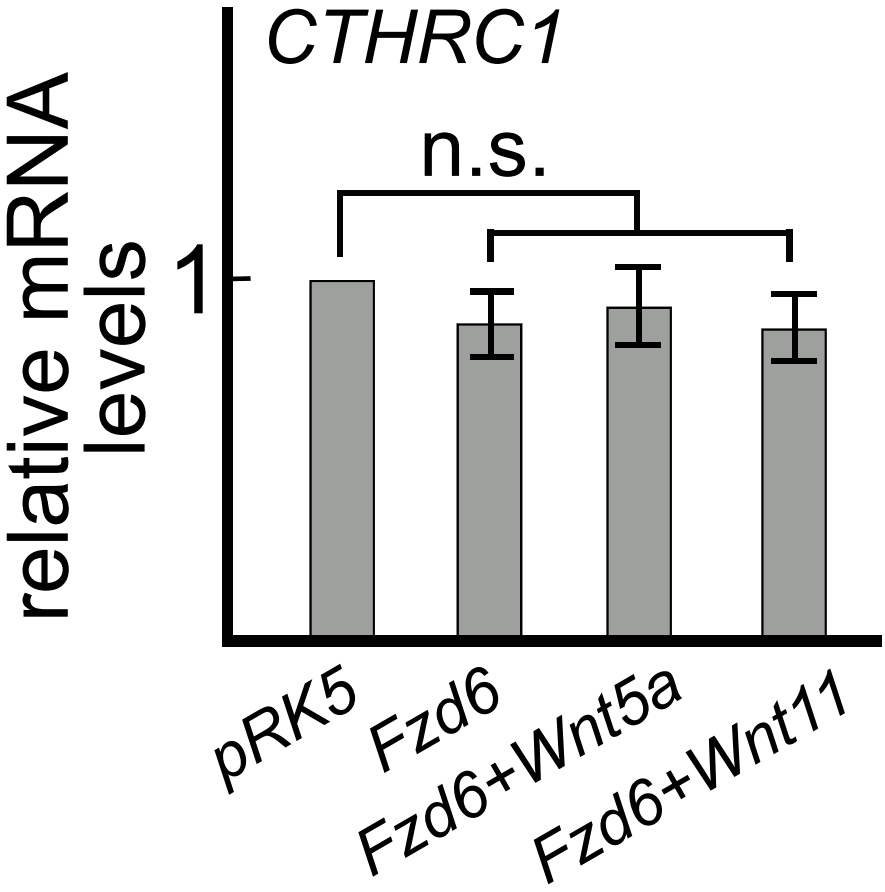

Figure S4. Transient expression of Fzd6 is not sufficient to drive *CTHRC1* expression *in vitro*. qRT-PCR shows no significant change in *CTHRC1* mRNA level in HEK293T cells transiently transfected with Fzd6, with or without the presence of recombinant Wnt5a or Wnt11 protein (100 ng/ml). All data represent mean ± SEM of three biological replicates. *GAPDH* was used as a control. Quantification of data was compared using ANOVA followed by Dunnett's test (n.s., not significant).

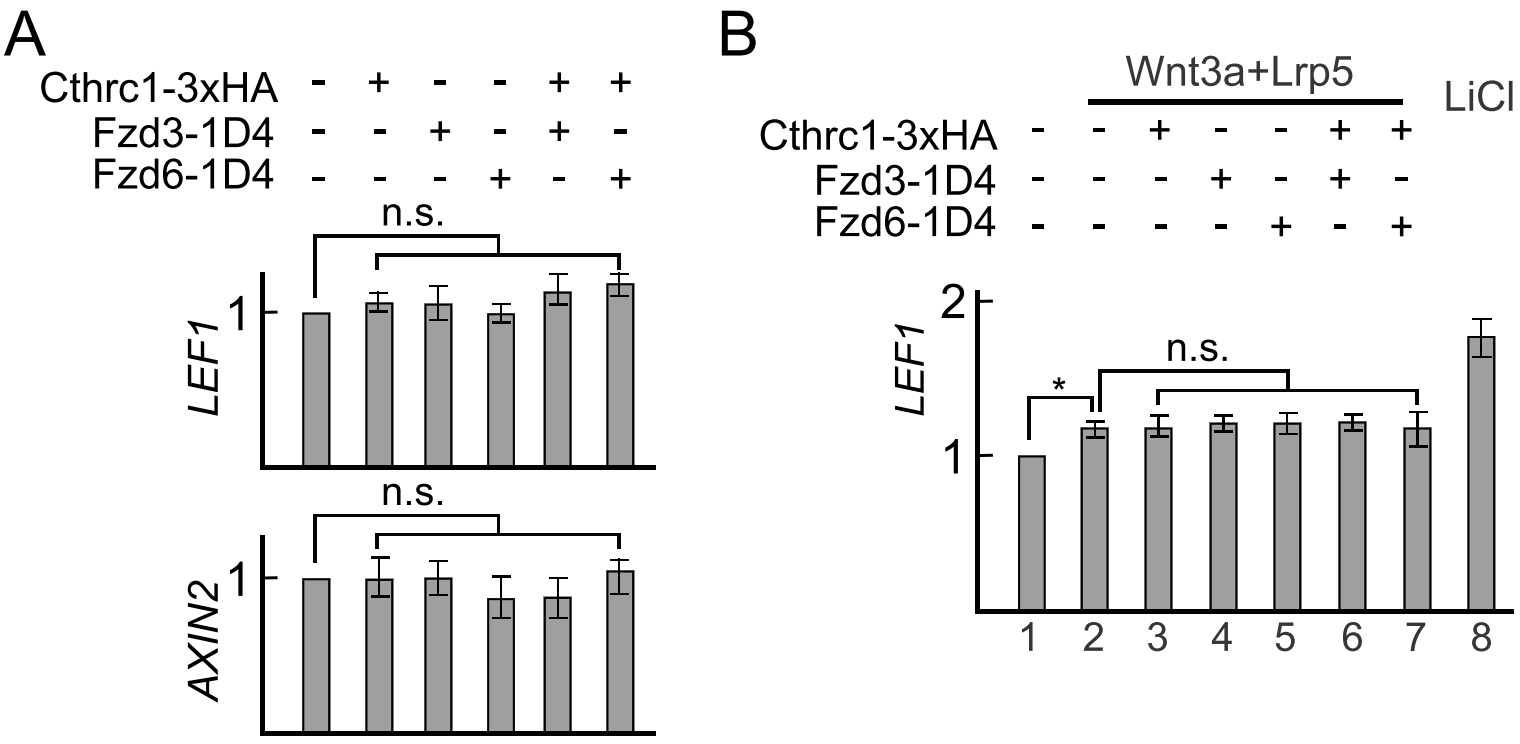

Figure S5. Cthrc1-Fzd3/6 does not affect canonical Wnt signaling pathway *in vitro*.

(A) Transient expression of Fzd3/6 only, Cthrc1 only, or both Fzd3/6 and Cthrc1 does not affect the basal level of canonical Wnt signaling in HEK293T cells, as qRT-PCR shows no significant changes in mRNA level of known canonical Wnt signaling targets (*LEF1* and *AXIN2*).

(B) Recombinant Wnt3a together with the transient transfection of Lrp5 induces a significant increase of *LEF1* expression in HEK293T cells (17%, column 2 vs. 1), as compared to the 20 mM LiCl treatment (76%, column 8 vs. 1). Transient expression of Fzd3/6 only, Cthrc1 only, or both Fzd3/6 and Cthrc1 does not affect the *LEF1* expression induced by Wnt3a+Lrp5. The data represent mean ± SEM of three biological replicates. *GAPDH* as a control. Quantification of data was compared using ANOVA followed by Dunnett's or Tukey's test (*, $P < 0.05$; n.s., not significant).

Table S1. Primers used for RT-PCR and quantitative real-time RT-PCR

Gene Symbol	Forward Primer	Reverse Primer
mFzd3	5′-ATGGCTGTGAGCTGGATTGTC-3′	5′-GGCACATCCTCAAGGTTATAGGT-3′
mFzd6	5′-ATGGAAAGGTCCCCGTTTCTG-3′	5′-GGGAAGAACGTCATGTTGTAAGT-3′
mSdc2	5′-TGTGTCCGCAGAGACGAGAA-3′	5′-GGAATCAGTTGGGATGTTGTCA-3′
mH21Rik	5′-TTTCAGCATTCCGGTGTCTTT-3′	5′-GGTGGGTAGTAGGGTGGAGAATA-3′
mGlipr2	5′-ATGGGCAAATCAGCTTCCAAA-3′	5′-GCTTCCCGGTTGAGCTTCTT-3′
mCthrc1	5′-CAGTTGTCCGCACCGATCA-3′	5′-GGTCCTTGTAGACACATTCCATT-3′
mSerhl	5′-ATGGGTTTGCACTCAGAGTTG-3′	5′-GCCAGCCGTGTAAGCAGAG-3′
mKrt13	5′-TCATCTCGGTTTGTCACTGGA-3′	5′-TGATCTTCTCGTTGCCAGAGAG-3′
mPsca	5′-GGACCAGCACAGTTGCTTTAC-3′	5′-GTAGTTCTCCGAGTCATCCTCA-3′
mGAPDH	5′-AGGTCGGTGTGAACGGATTTG-3′	5′-TGTAGACCATGTAGTTGAGGTCA-3′
hCTHRC1	5′-CAATGGCATTCCGGGTACAC-3′	5′-GTACACTCCGCAATTTTCCCAA-3′
hLEF1	5′-TGCCAAATATGAATAACGACCCA-3′	5′-GAGAAAAGTGCTCGTCACTGT-3′
hAXIN2	5′-TACACTCCTTATTGGGCGATCA-3′	5′-TTGGCTACTCGTAAAGTTTTGGT-3′
hGAPDH	5′-CTGGGCTACACTGAGCACC-3′	5′-AAGTGGTCGTTGAGGGCAATG-3′
hWNT1	5′-TTCAGACACGAGAGATGGAACT-3′	5′-CCAGCCTTCACTTGCTGAG-3′
hWNT2	5′-CCGAGGTCAACTCTTCATGGT-3′	5′-CCTGGCACATTATCGCACAT-3′
hWNT2B	5′-GGGGCACGAGTGATCTGTG-3′	5′-GCATGATGTCTGGGTAACGCT-3′
hWNT3	5′-CTCGCTGGCTACCCAATTTG-3′	5′-AGGCTGTCATCTATGGTGGTG-3′
hWNT3A	5′-AGCTACCCGATCTGGTGGTC-3′	5′-CAAACTCGATGTCCTCGCTAC-3′
hWNT4	5′-AGGAGGAGACGTGCGAGAAA-3′	5′-CGAGTCCATGACTTCCAGGT-3′
hWNT5A	5′-ATTCTTGGTGGTCGCTAGGTA-3′	5′-CGCCTTCTCCGATGTACTGC-3′
hWNT5B	5′-GCTTCTGACAGACGCCAACT-3′	5′-CACCGATGATAAACATCTCGGG-3′
hWNT6	5′-GGCAGCCCCTTGGTTATGG-3′	5′-CTCAGCCTGGCACAACTCG-3′
hWNT7A	5′-CTGTGGCTGCGACAAAGAGAA-3′	5′-GCCGTGGCACTTACATTCC-3′
hWNT7B	5′-CACAGAAACTTTCGCAAGTGG-3′	5′-GTACTGGCACTCGTTGATGC-3′
hWNT8A	5′-GAACCTGTTTATGCTCTGGGC-3′	5′-CAGCGTTCCCAAGCAAACTG-3′
hWNT8B	5′-CCGACACCTTTCGCTCCATC-3′	5′-CAGCCCTAGCGTTTTGTTCTC-3′
hWNT9A	5′-AGCAGCAAGTTCGTCAAGGAA-3′	5′-CCTTCACACCCACGAGGTTG-3′
hWNT9B	5′-TGTGCGGTGACAACCTCAAG-3′	5′-ACAGGAGCCTGATACGCCAT-3′
hWNT10A	5′-GGTCAGCACCCAATGACATTC-3′	5′-TGGATGGCGATCTGGATGC-3′
hWNT10B	5′-CATCCAGGCACGAATGCGA-3′	5′-CGGTTGTGGGTATCAATGAAGA-3′
hWNT11	5′-GGAGTCGGCCTTCGTGTATG-3′	5′-GCCCGTAGCTGAGGTTGTC-3′
hWNT16	5′-TTCAGACACGAGAGATGGAACT-3′	5′-CCAGCCTTCACTTGCTGAG-3′